Spectroscopy of the Cyano Radical in an Aqueous Environment

Piotr A. Pieniazek, Stephen E. Bradforth,* and Anna I. Krylov*

Department of Chemistry, University of Southern California, Los Angeles, California 90089-0482

Received: August 15, 2005; In Final Form: December 7, 2005

The effect of bulk water on the B $^2\Sigma^+ \leftarrow$ X $^2\Sigma^+$ and A $^2\Pi \leftarrow$ X $^2\Sigma^+$ electronic transitions of the cyano radical is investigated. First, the cyano radical−water dimer is characterized to understand the nature of the interactions and parametrize molecular mechanics (MM) potentials. The carbon atom, which hosts the unpaired electron, is found to have a Lennard-Jones radius smaller than typical force fields values. Classical molecular dynamics (MD) is then used to sample water configurations around the radical, employing two sets of MM parameters for the cyano radical and water. Subsequently, vertical excitation energies are calculated using time-dependent density functional theory (TD-DFT) and equation-of-motion coupled-cluster with single and double substitutions (EOM-CCSD). The effect of water is modeled by point charges used in the MD simulations. It is found that both bands blue-shift with respect to their gas phase position; the magnitude of the shift is only weakly dependent on the method and the MM parameter set used. The calculated shifts are analyzed in terms of the solute−solvent interactions in the ground and excited states. Significant contributions come from valence repulsion and electrostatics. Consequences for experiments on ICN photodissociation in water are discussed.

1. Introduction

Radicals in aqueous solutions play an important role in radiation chemistry and biology, heterogeneous atmospheric processes and are often implicated as enzymatic intermediates. However, the understanding of the electronic structure and spectroscopy of even simple radicals in water is very limited. This is due to the high reactivity of these species, which precludes experimental measurement of their spectra and properties. Of interest are the specific effects of a strongly interacting solvent such as water on the electronic structure of a solute, over and above classical dielectric solvation, on both the ground and particularly the excited electronic states. For example, charge transfer between solvent and solute can introduce new absorption bands. Furthermore, the degree of valence and Rydberg character in the isolated chromophore electronic transition can change markedly when the solute is embedded in a solution environment. Ironically, from the perspective of gas phase and matrix isolation electronic spectroscopy,[1] diatomic radicals (and diatomic molecules in general) are some of the most poorly characterized species[2] in terms of their visible and ultraviolet absorption bands once dissolved in water.

An excellent case in point is the cyano radical, CN, which is one of the most extensively studied radicals in the vapor phase due to its importance in combustion and astrophysics, as well as in fundamental reaction dynamics studies.[3−10] Its low lying electronic states are well-known through the "red" and "violet" absorption band systems where all rovibronic transitions have been cataloged into spectral atlases.[3,4] However, the electronic absorption spectrum of aqueous CN has never been reported. This poses considerable problems for a new generation of reaction dynamics studies exploring the role of the solvent on benchmark chemical reactions, e.g., the ICN photodissociation. Numerous theoretical studies have addressed how the environment affects energy dissipation, nonadiabatic curve crossing probabilities and the caging dynamics for this reaction, thus making it a most attractive system for calibrating theory with experiment.[11−16] Experimental work on this system in solution has begun to appear,[17−19] but uncertainty in spectral assignment of reaction products is currently hampering our progress toward a unified understanding of the reaction dynamics of this model system in solution. In particular, femtosecond studies probing reaction products near 390 nm have been assigned to CN (B $^2\Sigma^+ \leftarrow$ X $^2\Sigma^+$) by analogy to the gas-phase violet band.[18,20] On the other hand, Keiding's group monitoring the evolution of the full broadband spectrum developing after the reaction, instead assigned absorption near 390 nm to the I* product and a broad absorption band near 550 nm to CN.[21] Support for the latter assignment is provided by *ab initio* calculations for the CN/H_2O dimer.[21] The dramatically conflicting spectral assignments highlight the following: the magnitude and direction of the shift for the CN intramolecular B $^2\Sigma^+ \leftarrow$ X $^2\Sigma^+$ band is not known and the existence and location of any intermolecular charge-transfer (CT) band formed involving a neighboring water molecule, such as are observed for halogen radicals in water, has not yet been established.

Despite the simplicity of this or other diatomic radicals, *ab initio* theory has yet to provide help in this area. As can be seen for the case of CN detailed above, even the direction of the shift from vacuum can be in dispute. Rigorous theoretical description of solvent effects is one of the greatest challenges faced by *ab initio* methodology.[22−25] Indeed, every solvent molecule considerably increases the number of electronic and nuclear degrees of freedom. In view of the polynomial scaling of electronic structure methods, even the least computationally demanding electronic structure calculations, such as Hartree−Fock or density functional ones, become prohibitively expensive long before the bulk phase limit is reached. Moreover, averaging over solvent's nuclear degrees of freedom is required to compute experimentally relevant quantities. Fortunately, solvated species often retain their identity, which justifies separate treatment of the solvent and solute wave functions and describing the solvent effects as a perturbation. These ideas (based on the assumption that the solute electrons remain localized on the solute) have

10.1021/jp0545952 CCC: $33.50
Published on Web 03/18/2006

given rise to a plethora of solvation approaches, ranging from implicit solvent models to a variety of QM/MM methods.

The implicit solvent models (see ref 23 and references therein) are easily the least computationally expensive, as they do not include the solvent electronic or nuclear degrees of freedom. However, these methods suffer from two main drawbacks: (i) the inability to account for specific interactions, i.e., hydrogen bonding, and (ii) lack of information on the distribution of a given property.

If the solvent is included explicitly, as in QM/MM calculations, averaging over equilibrium solvent configurations, which can be performed using molecular dynamics (MD) or Monte Carlo techniques, requires many thousands of electronic structure calculations at different solvent configurations. Various levels of sophistication can be used to describe the solvent in QM/MM schemes. The simplest description of polar solvents is by a set of fixed point charges that emulate the electric field. Although very simple, this approach has been successfully used in the past to gain insight into the electronic structure of molecules in solution.[26−29] At the next level of sophistication one can include changes in electronic polarization in the ground and excited states of the solvent, as pioneered by Warshel and Levitt, who accounted for electronic relaxation.[30] Other researchers have explored different ways of coupling a solute to a polarizable MM solvent.[24,26,31,32] Although polarization effects may be dominant for nonpolar solvents, their relative contributions to electronic spectra in aqueous solutions are likely to be somewhat smaller. For example, Christiansen and co-workers, who studied the effect of water on the n $\rightarrow \pi^*$ transition in closed-shell formaldehyde,[33] have found that including polarization changes solvent induced shifts by less than 0.1 eV. Similar observations were reported by Gao for the n $\rightarrow \pi^*$ transition of pyrimidine.[26] Arguably, those effects might be stronger for the cyano radical because of a larger dipole moment change upon excitation. However, we expect that the electrostatic effects will remain dominant, as their magnitude is also proportional to the dipole moments values. The QM/MM description can be further improved by using an *ab initio* derived set of parameters to describe electrostatic, induction, and exchange interactions, as in the Effective Fragment Potential method by Gordon,[34,35] which was employed, among other applications, to study solvent-induced shifts in metalloprotein systems.[36]

In this paper, we apply a combination of MD and electronic structure calculations to predict and understand the first two valence absorption bands and their widths for the CN radical in water. The effect of water is modeled by a set of point charges. We chose this initial approach due to its simplicity and because the above-mentioned studies indicate a modest effect of solvent's electronic response on the spectral shift in aqueous solutions.

2. Methodology

2.1. Overview. The electronic spectrum of the aqueous cyano radical was simulated in a two step procedure. First, classical MD trajectories were launched to sample different thermally accessible configurations of water around the cyano radical. Intermolecular potentials were approximated by pairwise Lennard-Jones and charge−charge electrostatic terms, as detailed in section 2.3. Subsequently, vertical excitation energies of CN were computed by an electronic structure method, the solvent being described as point charges at positions from MD snapshots. The validity of this approach was tested on the CN···H_2O dimer, as is described in section 2.2. The *Amber*[37] package was used to perform MD simulations, whereas quantum calculations employed *Q-Chem*.[38] Additional calculations were performed using *ACES II*.[39]

TABLE 1: Ground-State Equilibrium Properties of the Cyano Radical Calculated at Different Levels of Theory Using the cc-pVTZ Basis Set

	r_e, Å	ν_e, cm^{-1}	μ, Debye
UHF	1.1505	2013	2.185
ROHF	1.1279	2453	2.285
UHF-MP2	1.1243	2908	2.149
ROHF-MP2	1.1882	1838	1.493
UHF−CCSD	1.1640	2178	1.522
ROHF−CCSD	1.1650	2158	1.468
ROHF−CCSD(T)	1.1753	2074	1.301
EOM-IP−CCSD	1.1636	2167	1.751
B3LYP	1.1627	2153	1.322
exp[a]	1.1718	2069	1.45

[a] Reference 1.

2.2. Cyano Radical−Water Dimer Calculations. Although seemingly simple, the gas-phase cyano radical requires an advanced level of theory for accurate description, as demonstrated by the results for various computational models summarized in Table 1. The unrestricted Hartree−Fock (UHF) solution exhibits a large spin-contamination, i.e., $\langle S^2\rangle_{UHF}$ is 1.075 instead of 0.75, as calculated using the cc-pVTZ basis. On the other hand, the restricted open-shell (ROHF) solution of the Hartree−Fock equations may be unstable due to the low lying B $^2\Sigma^+$ excited state at 3.195 eV vertically above X $^2\Sigma^+$. These problems with the reference adversely impact properties of the cyano radical at Hartree−Fock (HF) and second-order Møller−Plesset perturbation theory (MP2) levels. For instance, both dipole moments are above 2 D, as compared to the experimental value of 1.45 D.[40] The UHF-MP2 vibrational frequency is 2908 cm^{-1}, which is more than 40% higher than the experimental value. Only at the coupled-cluster with single and double substitutions (CCSD)[41] and the CCSD with perturbative account of triple excitations [CCSD(T)][42,43] levels are the experimental values for the gas-phase bond length, vibrational frequency, and dipole moment[1] closely matched. Noteworthy, at the CCSD level the reference has little impact on the quality of the ground-state results. However, the effects of spin-contamination in the reference on excited states can be more more pronounced.[44] To alleviate these problems, the ROHF references was used in all wave function calculations. Density functional theory (DFT) with the B3LYP[45] functional yields values comparable with CCSD results. In both cases, the agreement with experimental numbers is not quantitative. The aug-cc-pVTZ[46] and 6-311++G**[47,48] basis sets were used in the dimer ground-state calculations. Only the latter basis set was used to compute excitation energies for the dimer. Pure angular momentum d and f functions were employed.

The first part of this study focuses on the cyano radical−water interactions characterized by calculations on the CN···H_2O dimer. These calculations were used to derive Lennard-Jones parameters for the use in MD simulations, as well as assessed the accuracy of the method for simulating bulk phase spectra. Potential energy curves of the CN···H_2O dimer were calculated at the monomer gas-phase geometries shown in Figure 1. The distance between the fragments was varied from 2.00 and 2.25 Å up to 6.50 Å, for C_{2v} and C_s symmetry structures, respectively. Binding energies were obtained at the CCSD and CCSD(T) levels of theory. Basis set superposition error (BSSE) was accounted for by the counterpoise correction (CP).[49,50]

Vertical excitation energies from the X $^2\Sigma^+$ state to the $A^2\Pi$ and B $^2\Sigma^+$ states were calculated using the EOM-CCSD[51,52] as

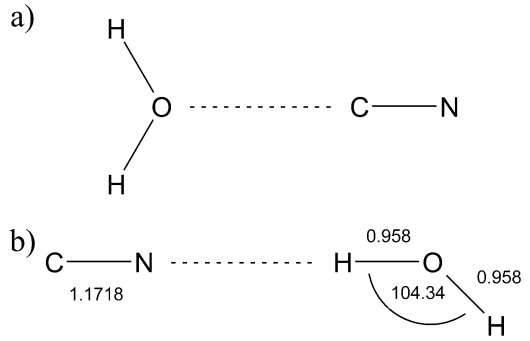

Figure 1. Geometries of the cyano radical−water dimer used for the PES scans. Monomers are frozen at their gas-phase geometries. Bond lengths are in Å and angles in degrees. (a) Planar C_{2v} structure. (b) C_s symmetry structure, C−N···H−O formation is collinear. The distance between the fragments was varied from 2.00 and 2.25 Å up to 6.50 Å, for C_{2v} and C_s symmetry structures, respectively.

well as TD-DFT[53] in the Tamm-Dancoff approximation[54] with the B3LYP functional.[45] Single-reference EOM-CC methods are particularly attractive for describing multiconfigurational excited states of the cyano radical because these methods (i) include both dynamical and nondynamical correlation in one computational scheme and (ii) describe several states of interest in a single calculation (not state-by-state). To validate our method of simulating bulk phase spectra, two types of dimer calculations were performed: (i) full quantum treatment of the dimer; (ii) the water molecule replaced by point charges located at hydrogen and oxygen atoms. Two sets of charges were employed: (i) reproducing the gas-phase dipole moment ($q_H = 0.328$);[55] (ii) charges from the SPC/E water model ($q_H = 0.4238$).[56]

To elucidate the degree of charge transfer between the cyano radical and water, the natural population analysis[57] was performed on the ground CCSD and the excited EOM-CCSD wave functions obtained using 6-311++G** basis set. This will provide hints as to the existence of a CT band in the condensed phase and allow an assesment of the classical description of the system, which assumes that there is no electron delocalization between water and the cyano radical.

2.3. Bulk Phase Calculations. The MD system consisted of 1000 water molecules (986 for TIP5P/E) and a cyano radical. SPC/E[56] and TIP5P/E[58] molecular mechanics models were used to simulate water. TIP5P/E is a version of Jorgensen's TIP5P model[59] re-optimized for use with Ewald summation. All simulations were performed in the isothermal−isobaric ensemble (constant T, P, N). Temperature was kept constant at 298 K using the weak-coupling algorithm,[60] with a time constant of 3 ps. A pressure variant of weak-coupling algorithm with isotropic position scaling was used to keep pressure constant at 1 atm. Barostat time constant was set to 3 ps. All bonds were constrained during the dynamics using the SHAKE algorithm with tolerance of 10^{-6} Å. Equations of motion were integrated using a 1 fs time step. Long-range interactions were handled using Ewald summation and a cutoff of 8 Å was applied to the Lennard-Jones interactions. Periodic boundary conditions were applied. Quantum mechanical calculations of the cyano radical in the electric field of point charges were performed in the cc-pVTZ basis set.

The interaction of the cyano radical with water in the MD simulations was modeled by a sum of 6-12 Lennard-Jones and charge−charge electrostatic terms. SPC/E parametrization was used to model water in derivation of charges. The interaction sites of the cyano radical were on carbon and nitrogen. Lorentz−Berthelot mixing rules were used to obtain interaction parameters between different atom types. Two sets of Lennard-Jones parameters used in calculations are given in Table 2. Set A is taken from the *Amber* force field,[61] Set B was derived from the dimer calculations ($CN\cdots H_2O$). The atomic charges for CN were derived by the following self-consistent procedure. Starting with the initial guess of 0.400, with the carbon atom bearing the positive charge, and for each set of Lennard-Jones parameters, three trajectories were allowed to equilibrate for 500 ps, followed by a production run of 150 ps. Snapshots were taken every 1 ps. At each snapshot the dipole moment of the cyano radical was calculated using CCSD/cc-pVTZ. New charges were hence derived to reproduce the average dipole moment. Then the system was allowed to equilibrate for 150 ps with the new set of charges, followed by another production run. The procedure was repeated until the change in charge was less than 0.001. This required five iterations for set A and six iterations for set B. The obtained charges are listed in Table 2. The dipole moment increased from 1.45 D in the gas phase to 2.05 D in water. No re-optimization was performed for simulations employing the TIP5P/E model.

TABLE 2: Lennard-Jones and Electrostatic Interaction Parameters for $CN\cdots H_2O$[a]

	ϵ_C, kcal/mol	σ_C, Å	ϵ_N, kcal/mol	σ_N, Å	q_C
set A	0.086	3.40	0.170	3.25	0.3648
set B	0.089	2.60	0.180	3.32	0.3632

[a] Set A has been taken from the *Amber* force field and set B has been developed in this work.

A total of three different bulk phase model systems was simulated: (i) set A + SPC/E, (ii) set B + SPC/E, and (iii) set B + TIP5P/E. For each system, five MD trajectories were launched using random initial velocities and positions (molecules were placed on a simple cubic lattice and then rotated by the three Euler angles sampled from a uniform distribution). Each trajectory was allowed to equilibrate for 500 ps. This was followed by a 200 ps production run with snapshots taken every 1 ps. At each snapshot, vertical excitation energies were computed using EOM-CCSD/cc-pVTZ. Additionally, for model system (iii) the energies were computed using TD-DFT/B3LYP/cc-pVTZ. The local structure of water around the cyano radical was analyzed by means of radial and angular distribution functions.

3. Results and Discussion

3.1. Cyano Radical−Water Dimer. In the X $^2\Sigma^+$ ground state the cyano radical has a dipole moment of 1.45 D, the carbon atom bearing the positive charge and the unpaired electron.[40] On the basis of electrostatic considerations, the two configurations of the cyano radical−water dimer presented in Figure 1 were selected for potential energy surface (PES) scans. These scans represent the two limiting interaction scenarios between the monomers. One corresponds to a negatively charged oxygen atom interacting with the positively charged carbon atom. This gives rise to the planar C_{2v} complex. The C_s structure represents a hydrogen bonding situation, in which the negatively charged nitrogen atom acts as a hydrogen bond acceptor. Frequency calculations carried out near the minima reveal that the C_s structure is, in fact, a minimum, whereas the C_{2v} structure has three imaginary frequencies (160, 66, and 65 cm^{-1}), corresponding to out-of-plane hydrogen wag, out-of-plane CN wag, and in-plane antisymmetric pseudorotation of the monomers, respectively. We retained this structure because it captures the essentials of the carbon−oxygen interaction and provides the simplicity needed in the analysis of dimer properties and force field parametrization.

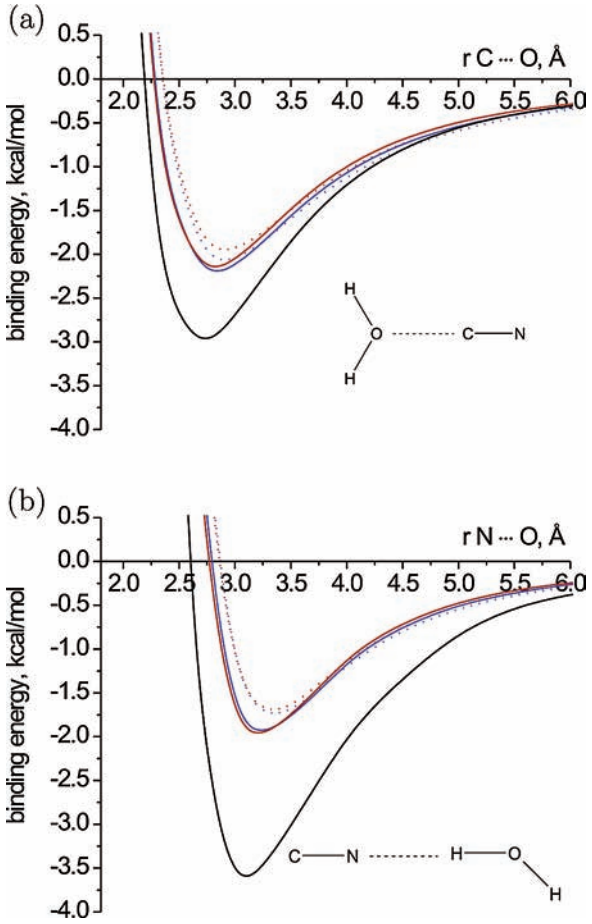

Figure 2. CP corrected dimer potential energy curves along interfragment separation coordinate. (a) C_{2v} symmetry structure. (b) C_s symmetry structure. The energies were obtained at the CCSD/6-311++G** (blue dotted line), CCSD(T)/6-311++G** (red dotted line), CCSD/aug-cc-pVTZ (blue solid line), and CCSD(T)/aug-cc-pVTZ (red solid line line) levels of theory. For comparison, the CCSD(T)/aug-cc-pVTZ scan without BSSE correction is shown (solid black line).

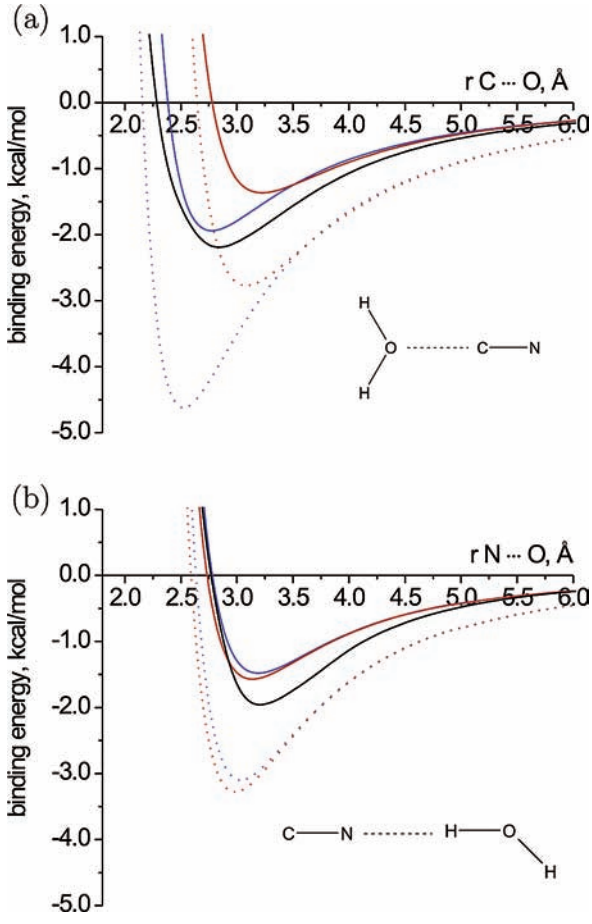

Figure 3. Comparison of the *ab initio* and molecular mechanics dimer potential energy surfaces. (a) C_{2v} symmetry structure. (b) C_s symmetry structure. The energies were obtained using: CCSD(T)/aug-cc-pVTZ (black solid line), *Amber*'s Set A and SPC/E Lennard-Jones parameters with charges reproducing gas phase dipole moments (red solid line) and condensed phase charges (red dotted line), newly derived Set B and SPC/E Lennard-Jones parameters with charges reproducing gas-phase dipole moments (blue solid line) and condensed phase charges (blue dotted line).

First, let us look at the strength of CN ···H_2O interaction and the range of resulting intermolecular separations. Figure 2 presents the CP corrected scans of PES, as well as a single curve without the CP correction. The general effect of the CP correction is an increase of the minimum energy distance (r_e) and a decrease of the complex dissociation energy (D_e). Surprisingly, perturbative inclusion of triple excitations results in only minor changes of CCSD PES. The basis set dependence is more pronounced—larger basis set yields stronger binding. The minimum along the C_s curve is located around 3.25 Å. The CCSD(T)/6-311++G** binding energy is 1.70 kcal/mol. Increasing the basis set to aug-cc-pVTZ increases D_e to 1.95 kcal/mol. The respective, before BSSE-correction, values are 2.20 and 3.46 kcal/mol. These can be compared to the corresponding value for the hydroxyl radical, which is 2.40 kcal/mol at the CCSD(T)/6-311++G(2d,2p)//B3LYP/6-311++G(2d,2p)[62] (without the BSSE correction). The C_{2v} structure exhibits a minimum at about 2.75 Å. The CCSD(T) binding energy increases from 1.83 to 2.15 kcal/mol upon increasing the basis set size. Values without the BSSE correction are 2.82 and 2.93 kcal/mol, respectively. Again, the corresponding value for the hydroxyl radical is 5.87 kcal/mol.[62] The large difference cannot be accounted for by pure electrostatics, as the dipole moment of the hydroxyl radical is 1.668 D and that of the cyano radical 1.45 D.[1] Rather, this is a signature of hydrogen bonding, where the OH group is a hydrogen donor. Overall, although the cyano radical interacts quite strongly with water, it is a weaker hydrogen bond acceptor than OH. The latter is very fortunate, as such an interaction is likely to affect the spectrum beyond electrostatics and is not easily incorporated into bulk phase calculations.

The above *ab initio* PES scans can be used to derive interaction parameters and assess the quality of the MM CN···H_2O potential, which is approximated by pairwise 6-12 Lennard-Jones and charge−charge electrostatic energy terms. Polarization and electron delocalization effects, which become important at short intermolecular separations, are absent in the MD model. To ensure an unambiguous comparison, charges for the gas-phase potential were fitted so as to reproduce the gas-phase dipole moments of the cyano radical and water: 1.45 and 1.855 D,[55] respectively (the corresponding charges are 0.258 for carbon and 0.3285 for hydrogen). Individual fragments are kept neutral. Two sets of Lennard-Jones parameters were tested. Set A employs the values from the *Amber* force field.[61] Set B was derived by fitting to the *ab initio* scans of dimer PES. The parameters are presented in Table 2, and the potentials are plotted on Figure 3. The potential for C_s PES scan is well reproduced using typical Lennard-Jones radii. Consequently, only minor adjustments were made to nitrogen parameters. The interaction on the carbon side, where the unpaired electron is

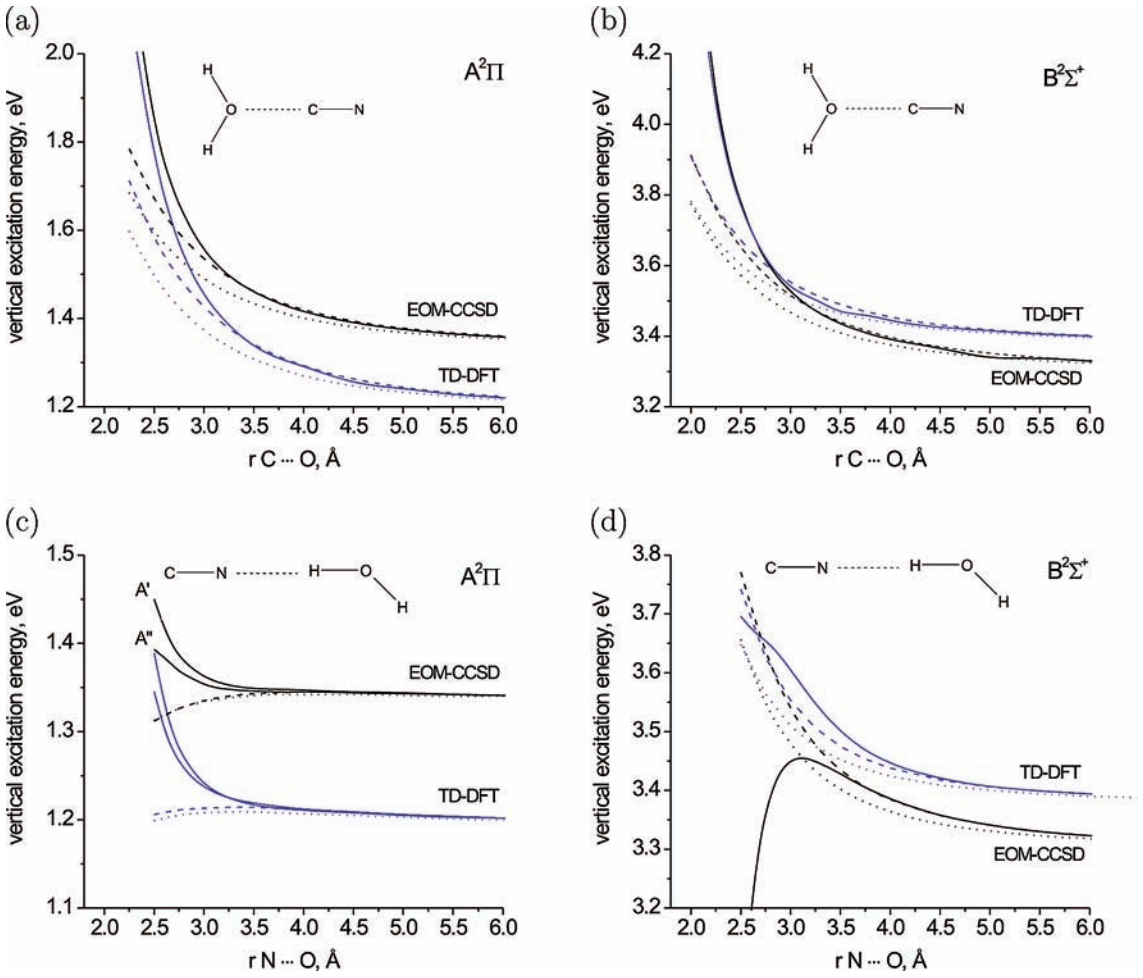

Figure 4. Vertical excitation energies as a function of monomer separation calculated by full EOM-CCSD (black solid line), full B3LYP (blue solid line). Results of calculations with water replaced by point charges reproducing the water gas-phase dipole moment (EOM-CCSD, black dotted line; B3LYP, blue dotted line) and charges used in SPC/E water model (EOM-CCSD, black dashed line; B3LYP, blue dashed line) are also shown. Panel (a) the $A^2\Pi$ state along the C_{2v} scan (only the in-plane B_1 component is shown, as the B_2 component is nearly degenerate), (b) the B $^2\Sigma^+$ state along the C_{2v} scan, (c) the $A^2\Pi$ state along the C_s scan (both the A′ and A″ components are shown), (d) the B $^2\Sigma^+$ state along the C_s scan.

located, was more problematic. Typical force field radii make the carbon atom too big. On the other hand, a much smaller value leads to overestimation of potential well depth due to the electrostatic collapse. The position of the Lennard-Jones hard wall may have a significant effect on the calculated spectra, because at short distances water has the most dramatic effect on vertical excitation energies, as can be seen in Figure 4. For instance, in the C_{2v} structure the excitation energy changes by 0.3 eV when the intermolecular distance decreases from 2.50 to 2.25 Å. This distance change corresponds roughly to the shift in the carbon−oxygen radial distribution functions obtained using the two parametrizations. Consequently, deriving a CN specific parameter set is justified.

Having described the ground-state intermolecular potential, we now proceed to the excited states of the cyano radical in the dimer. The two excited states of the cyano radical that are of interest here are the valence $A^2\Pi$ and B $^2\Sigma^+$ states, corresponding to the $\pi \rightarrow n_C$ and $n_N \rightarrow n_C$ excitations, respectively. The oscillator strength associated with those transitions are 0.0034 and 0.033, respectively.[1] Both excitations result in a change of the direction of the dipole moment relative to ground state (1.45 D), which is 0.56 D in $A^2\Pi$ and 1.15 D in B $^2\Sigma^+$ state (nitrogen atom bears the positive charge).[40,63] EOM-CCSD using 6-311++G** basis predicts dipole moments of 0.33 and 1.45 D, respectively. The calculated oscillator strength are 0.0032 and 0.039 for the A and B states, respectively.

The accuracy of our bulk phase spectra can be assessed by considering the effect of replacing water by point charges in the dimer calculations. These and full quantum excitation energies computed as a function of distance between the monomers using EOM-CCSD and TD-DFT B3LYP are presented in Figure 4. The TD-DFT energies are systematically lower than the corresponding EOM-CCSD values for the transition to the $A^2\Pi$ state and higher for the B $^2\Sigma^+$ state transition. Further analysis considers the C_{2v} and C_s scans separately.

Water approaching the cyano radical from the carbon side increases the energy gap between the ground and excited states (Figure 4a,b). The dependence on the distance is particularly strong in the region below 3 Å. The splitting of $A^2\Pi$ into the $^2B_1$ and $^2B_2$ states in C_{2v} is rather small, e.g., 0.01 eV at 2.75 Å; therefore only the higher energy component $^2B_1$ is shown (in-plane). EOM-CCSD and TD-DFT are in qualitative agreement. When water is replaced by point charges, slightly lower excitation energies are observed, but the trends are reproduced correctly.

A more complicated behavior is observed when water is located on the nitrogen end of the cyano radical (Figure 4c,d). Full EOM-CCSD calculations reveal that the B $^2\Sigma^+ \leftarrow$ X $^2\Sigma^+$ transition energies fall dramatically after a small initial rise. The

excitation energies to $A^2\Pi$ increase at shorter distances. Moreover, around 2.75 Å splitting of this level into the A′ and A″ components in the C_s symmetry becomes significant. B3LYP incorrectly predicts that the B $^2\Sigma^+ \leftarrow$ X $^2\Sigma^+$ transition energies will increase at short distances but correctly describes the behavior of the $A^2\Pi$ state. When charges are used to represent water, the separation between the ground and the B $^2\Sigma^+$ states increases at short distances, in disagreement with the full EOM-CCSD treatment. The transitions to the $A^2\Pi$ state occur at lower energies relative to the full quantum mechanical treatment, regardless whether EOM-CCSD or TD-DFT is used to treat the radical. Fortunately, the discrepancies between the quantum and electrostatic treatments of water become significant only in the region below 2.75 Å. Nitrogen−oxygen radial distribution functions calculated from MD trajectories essentially vanish at this distance, which means that these configurations are not sampled at equilibrium conditions. This is consistent with the condensed phase dimer potential, as it becomes strongly repulsive at this distance resulting in low Boltzmann weights of those configurations.

To summarize, our model, in which water is described by point charges, can quantitatively reproduce the excitation energies of the cyano radical in the CN···H_2O dimer at large and intermediate distances. Another interesting issue is the character of the electronic states of the dimer. For example, both the ground state and the excited state may acquire significant charge transfer character in water and will consequently require explicit water molecules in the quantum calculation. Natural population analysis allowed us to assess the degree of charge transfer between the monomers. The natural charge on the cyano radical as a function of monomer separation is shown in Figure 5. For both geometries under scrutiny charge transfer occurs at distances below 3.25 Å. In the ground-state C_s structure the cyano radical acquires a partial positive charge; charge is pulled from the negative nitrogen atom by the positive hydrogen atom. When the system is excited to the B $^2\Sigma^+$ state (nitrogen becomes positive), the charge flows back from water to the radical making it negative, which is consistent with the dipole moment flip upon excitation. Components of the $A^2\Pi$ state are also characterized by a positive charge on CN. This is surprising, as in this state the dipole moment also flips relative to ground state and the nitrogen is positive, though its magnitude is smaller than that in the B $^2\Sigma^+$ state. This is possibly due to the concomitant delocalization of the π cloud across the hydrogen bond. In the C_{2v} structure there is a charge flow to the radical in the ground state, oxygen donates its electrons to the carbon atom. Excitation to the B $^2\Sigma^+$ state leads to depletion of the net charge on the cyano radical; however, it remains negative. The $A^2\Pi$ state exhibits only minor charge transfer and the monomers are neutral. Overall, appreciable amount of charge transfer occurs only at very short monomer separations, i.e., 2.5 Å for C_{2v} structures and 2.75 Å for C_s structures. It is at those distances that the intermolecular potentials become strongly repulsive and the radial distribution functions essentially vanish. Thus, at configurations sampled in bulk water simulations, the valence electronic states of the cyano radical preserve their gas-phase identity in the condensed phase and our method describes them correctly. However, it is reasonable to expect that a CT state may appear in water, in addition to the two valence excited states of the cyano radical.

3.2. Bulk Phase Calculation. In this section, we first analyze the structure of water around the cyano radical, focusing mostly on differences between force field parametrizations. Then we proceed to the analysis of the calculated electronic excitation spectra.

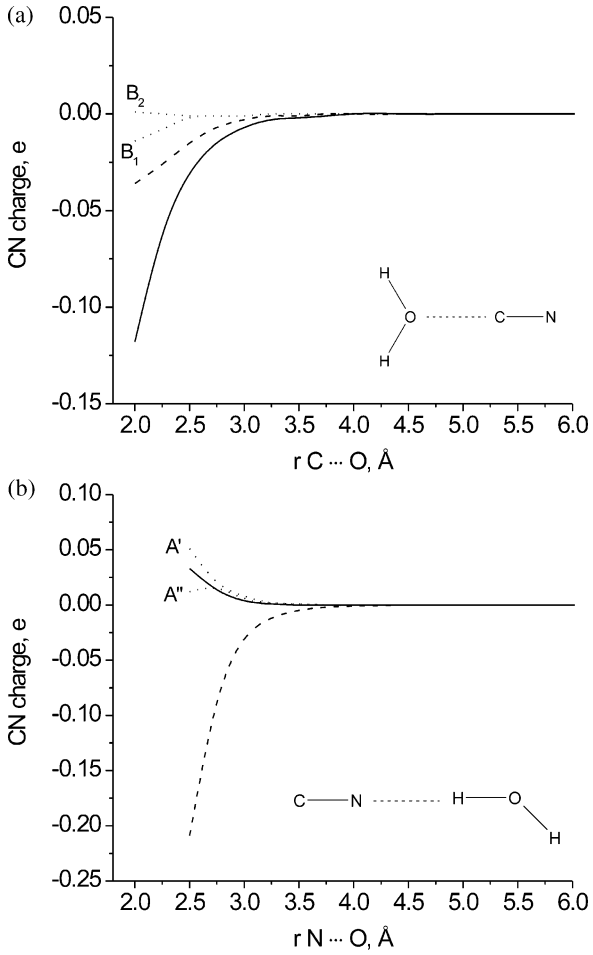

Figure 5. Natural charge of the cyano radical in the ground and excited states of the cyano radical−water dimer. The CCSD/6-311++G** and EOM-CCSD/6-311++G** wave functions are analyzed along C_{2v} and C_s scans, panels (a) and (b), respectively. The X $^2\Sigma^+$ ground state (solid line), the B $^2\Sigma^+$ state (dotted line), and the $A^2\Pi$ state (dashed line).

3.2.1. Local Solvent Structure around the CN Radical. General features of the solvent structure around the solute are given by the radial distribution functions between the geometric center (GC) of the cyano radical and water oxygen (OW) and hydrogen (HW), which are plotted in Figure 6. Overall, they exhibit little dependence on the water model employed. The GC−OW plot exhibits a shift to larger distance of the first peak on the distribution function obtained using set A of Lennard-Jones parameters with respect to the newly derived set B by ca. 0.2 Å, consistent with relative sizes of the carbon atom in the two sets. A similar effect is observed in GC−HW distribution functions. This is surprising, because there is very little difference between the parameters of the nitrogen atom, where one expects to find the closest hydrogen atom. There is essentially no shift in the nitrogen−hydrogen radial distribution function (not shown), which suggests that this effect is due to hydrogen atoms located on the side of the cyano radical.

Due to the angular averaging, radial distribution functions provide a relatively crude description of the solvent structure. A closer look at the immediate vicinity of the cyano radical is desired, because it is those molecules that have the strongest effect on the electronic spectrum. One useful parameter is the coordination number as determined by the integration of the radial distribution function. Two upper integration bounds were

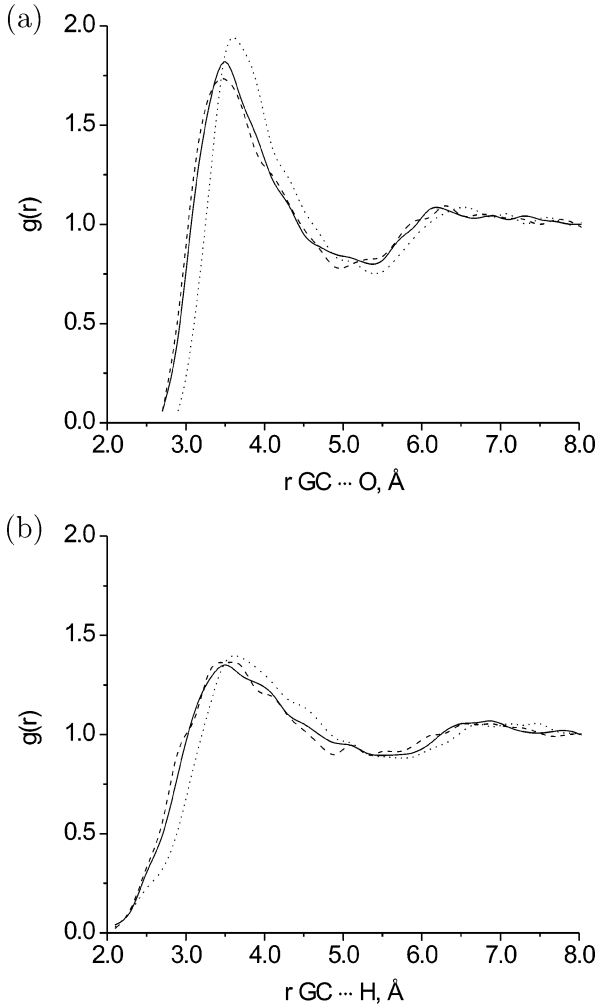

Figure 6. Radial distribution functions of oxygen (a) and hydrogen (b) around the geometric center of the cyano radical. The bin size is 0.2 Å. The curves are set B + SPC/E (solid line), set A + SPC/E (dotted line), set B + TIP5P/E (dashed line).

TABLE 3: Basic SPC/E and TIP5P-E Water Model Parameters

	SPC/E	TIP5P/E
q_H	0.4238	0.2410
σ, Å	3.166	3.097
ϵ, kcal/mol	0.1553	0.178
r_{OH}, Å	1.0	0.9572
θ_{HOH}	109.47	104.52

TABLE 4: Coordination Number of Cyano Radical in Water Using Different Definitions of the First Solvation Shell

	r,[a] Å	N_1[b]	N_2[c]
set B + SPC/E	3.55	3.84	16.64
set A + SPC/E	3.70	4.24	16.89
set B + TIP5P/E	3.45	3.16	16.64

[a] Maximum on the geometric center of CN−oxygen radial distribution function. [b] Number of water molecules closer than the maximum on the radial distribution function. [c] Number of water molecules closer than 5.1 Å.

used: (i) the first maximum on GC−OW radial distribution function and (ii) 5.1 Å, where the first minimum is located. The results are summarized in Table 4. Overall, it appears that 16 water molecules are needed to fully surround the cyano radical by a shell of water. This result is rather insensitive to the potential used for the cyano radical, because the long-range structure of solution is defined primarily by the water−water potential. There are ca. 3.5 nearest-neighbor water molecules. *Amber*'s set A, with a slightly larger carbon radius, yields a larger number of nearest neighbors. The difference between the SPC/E and TIP5P/E results is largely due to the uncertainty in the determination of the maximum of the radial distribution function and a strong dependence on the cutoff radius.

We can further investigate positions of the four nearest neighbors by means of angular probability distribution functions. The angular variable is the angle between N−C and GC−OW (HW) vectors; e.g., zero corresponds to the oxygen (hydrogen) atom located on the CN axis at the carbon atom end. The radial limits were chosen to include one, two, three, and four nearest oxygen (hydrogen) atoms. Overall, the angular probability distributions exhibit stronger dependence on the force field for the cyano radical than the radial distribution functions. The first oxygen atom is located preferentially on the side of the cyano radical (ca. 90°). The angle is smaller for newly derived set B, meaning that the oxygen is closer to the carbon. This is a direct consequence of the smaller Lennard-Jones radius, which allows for a stronger electrostatic interaction. As the radial range is extended to include more water molecules, the distribution for *Amber*'s set A and SPC/E water becomes broader, the maximum remaining at approximately 90°. On the other hand, when the radial range is extended for set B, featuring a smaller carbon atom, the probability distribution develops a shoulder at smaller angles, meaning that the successive oxygen atoms are located preferentially near carbon. The angular distribution of the first hydrogen show the presence of the hydrogen atom on the CN axis near nitrogen thus indicating a hydrogen bond. Subsequent hydrogen atoms are likely to be found alongside of the cyano radical. The dependence on both the water model and the cyano radical parametrization is stronger for the angular distribution of hydrogen than that of oxygen.

Overall, the averaged structure of the first solvation shell of the cyano radical is barrel-like. The nearest water molecules are located alongside of CN and the whole structure is capped on both ends. The position of the capping water on the nitrogen end is consistent with a hydrogen bond. Note that the definition of coordination sphere used here is biased toward water molecules located alongside of the cyano radical, because it is defined with respect to the geometric center of CN. The observed structural differences between different parametrizations are not qualitative and can be easily understood on the basis of the parametrization of the CN radical, although they may still lead to different dynamics of the cyano radical. Moreover, including water explicitly in the quantum calculation of electronic spectrum would yield stronger dependence on the angular distribution of water, because orbital overlap has a stronger directional character than electrostatic interactions.

3.2.2. Electronic Spectrum of the Aqueous Cyano Radical. The interaction between water molecules and the cyano radical is different in the CN ground and excited states, the strength of the interaction varying with the geometry of the system. In the present study we sample different configurations of water, thus accounting for the inhomogeneous broadening part of the electronic spectrum. The spectra are presented in Figure 8, and the band parameters are listed in Table 5. Overall, the centers of the bands are blue-shifted relative to the calculated gas-phase position (1.327 and 3.347 eV for the $A^2\Pi \leftarrow X\ ^2\Sigma^+$ and the $B\ ^2\Sigma^+ \leftarrow X\ ^2\Sigma^+$ transition, respectively, at the EOM-CCSD/cc-pVTZ level), regardless of a MD or an electronic structure model. The widths are ca. 0.4 and 0.14 eV for the B and A bands, respectively. The relative insensitivity of the calculated

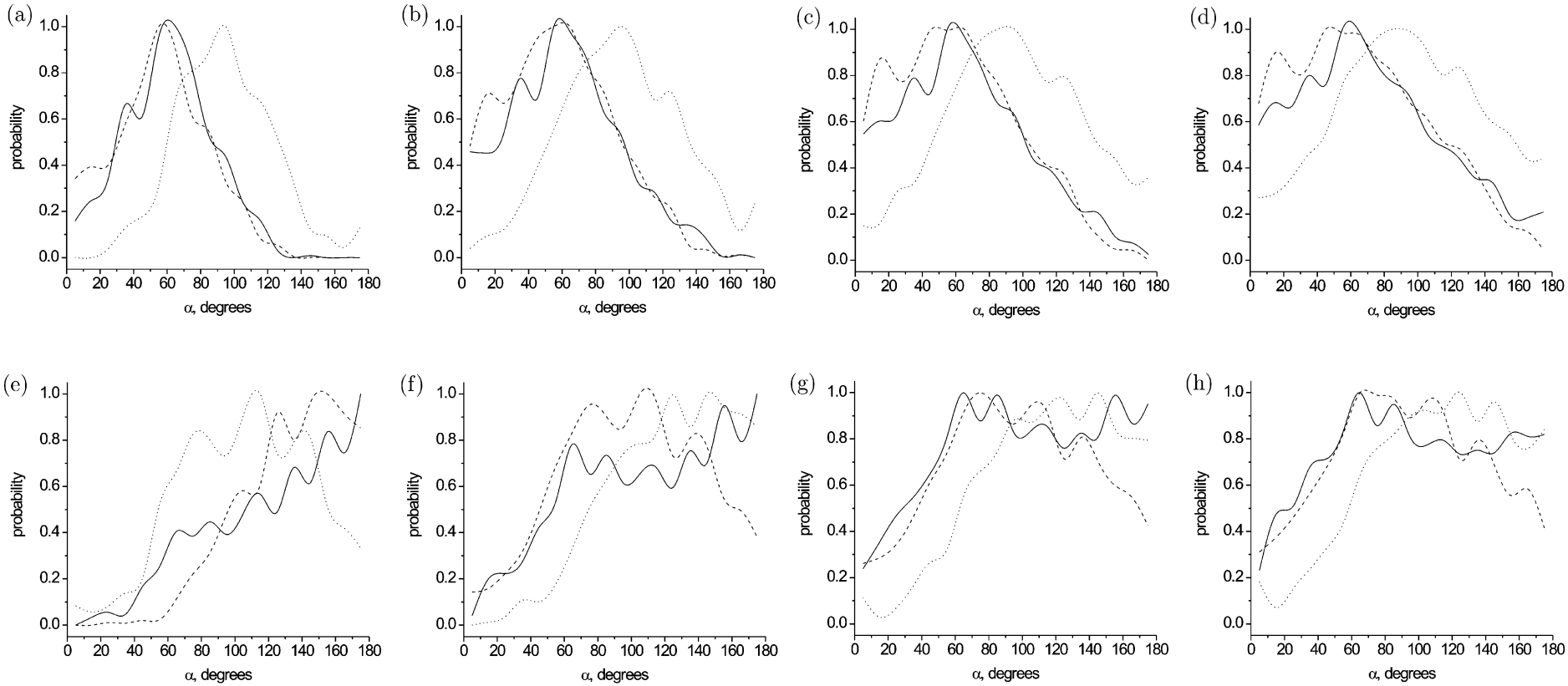

Figure 7. Angular distribution of oxygen (a)−(d) and hydrogen (e)−(h) around the cyano radical. The angular variable is the angle between CN and the geometric center−oxygen (hydrogen) vectors. Radial range is successively increased to include between one and four atoms. The curves are set B + SPC/E (solid line), set A + SPC/E (dotted line), set B + TIP5P/E (dashed line).

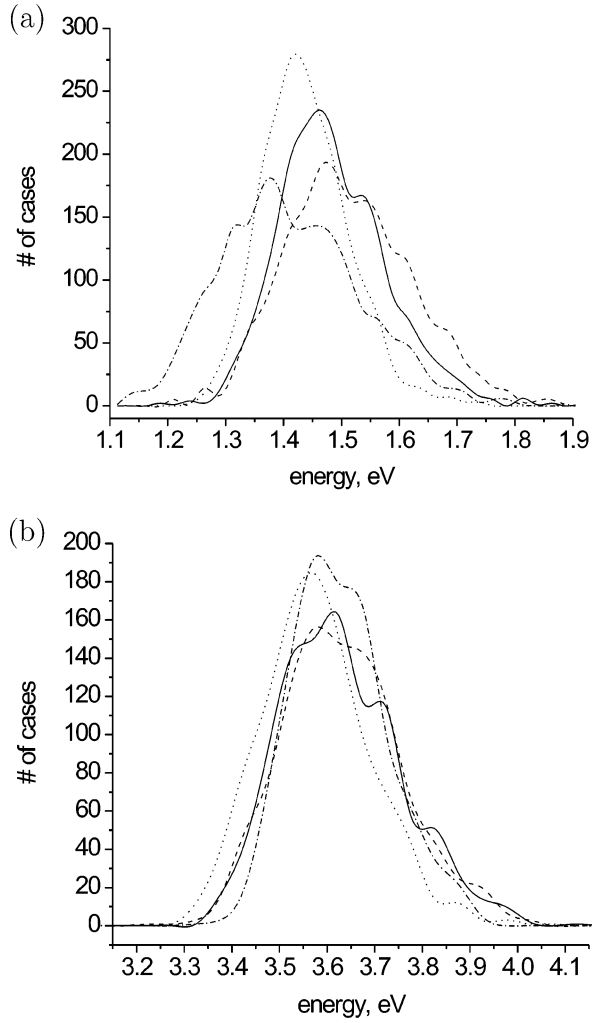

Figure 8. Simulated spectra of the cyano radical in water: (a) the A ← X transition; (b) the B ← X transition. The spectra are set B + SPC/E (solid line), set A + SPC/E (dotted line), set B + TIP5P/E (dashed line), set B + TIP5P/E +TD-DFT/cc-pVTZ. Unless otherwise indicated the energies were computed using EOM-CCSD/cc-pVTZ (dash−dot line). Wiggles are a result of a finite sample of excitation energies.

TABLE 5: A ($A^2\Pi \leftarrow X\ ^2\Sigma^+$) and B ($B\ ^2\Sigma^+ \leftarrow X\ ^2\Sigma^+$) Band Parameters

	set B + SPC/E	set A + SPC/E	set B + TIP5P/E	set B + TIP5P/E + TD-DFT
		A Band ($A^2\Pi \leftarrow X\ ^2\Sigma^+$)		
$\nu_0{}^a$	1.47	1.43	1.50	1.40
$\nu_{1/2}{}^b$	0.30	0.24	0.37	0.41
$\Delta\nu^c$	0.14	0.10	0.18	0.07
$\nu_s{}^d$	0.061	0.057	0.059	0.061
		B Band ($B\ ^2\Sigma^+ \leftarrow X\ ^2\Sigma^+$)		
$\nu_0{}^a$	3.61	3.57	3.62	3.61
$\nu_{1/2}{}^b$	0.42	0.37	0.42	0.34
$\Delta\nu^c$	0.26	0.22	0.27	0.27

[a] Position of the band center, eV. [b] Full width at half-maximum, eV. [c] Blue shift relative to gas-phase position, eV. [d] Splitting of the A $^2\Pi$ level, eV.

spectra to the water model employed is consistent with the radial distribution functions that are very similar for both models, which means that the point charges are positioned in similar range. The particular choice of the water model has a greater impact on the A $^2\Pi \leftarrow X\ ^2\Sigma^+$ than on the B $^2\Sigma^+ \leftarrow X\ ^2\Sigma^+$ transition, as observed in both the corresponding shifts and widths. Next, the spectra obtained using *Amber*'s set A are systematically slightly narrower and less blue-shifted. This is because water in this model is farther away on average from the cyano radical. Overall, the differences between the calculated spectra are much smaller than their widths. Thus, we conclude that our model is rather robust and the effect on the absorption spectrum is insensitive to the variation of the parameters within the uncertainty range.

As observed in the dimer calculations, TD-DFT yields reliable results (as compared against EOM-CCSD) when charges are used to model the effect of water. To test how big the difference between the two methods is in the bulk phase, we performed TD-DFT calculations for the trajectory utilizing the newly derived set B and TIP5P/E water. The density functional results for individual snapshots are, on average, shifted to the red by 0.102 ± 0.012 eV for A band and 0.005 ± 0.026 eV for B band as compared to the EOM-CCSD results. Thus, essentially identical shifts are obtained at a much lower cost, which suggests that one could employ TD-DFT in calculations of spectroscopic correlation function necessary for computing homogeneous and inhomogeneous contributions to the bandwidth. Such calculations require calculating excitation energies along the equilibrium trajectories at very small time steps for extended periods to ensure appropriate sampling. However, we note that TD-DFT is not a viable approach for including explicit water molecules into the quantum calculation, because charge transfer excitations are incorrectly described by TD-DFT. Those states artificially mix with valence excited states and neither type of states is described correctly.[64] Indeed, in a cluster calculation with four water molecules, it was impossible to assign any valence excited states of the cyano radical.

3.2.3. Nature of CN−Water Interactions and Their Contributions in the Spectral Shifts. Let us analyze the calculated spectra in the context of first principles solvation ideas, following the discussion by Bayliss and McRae.[65] We neglect here any geometrical changes in the CN radical. This seems justified due to high vibrational frequency of the bond. In solutions, the electronic states of a solute are modulated by the surrounding solvent molecules, making them as well as the excitation process more complex than in the gas phase. The main interactions are: (i) electrostatics, (ii) dispersion, and (iii) valence repulsion (referred to as packing strain in the original paper). Those interactions give rise to an equilibrium cage structure of a polar solvent around a polar solute. Upon excitation, a Franck−Condon excited state is formed (i.e., the electronic distribution changes) whereas the nuclear degrees of freedom remain frozen. As a result, the aforementioned interactions will be different in the excited and the ground states giving rise to a spectral shift. Below we discuss the relative importance of those factors for the cyano radical−water system and whether the observed shift is due to the ground-state stabilization or the excited-state destabilization.

Because for the problem at hand both the solute and the solvent are polar, one may expect that electrostatics will dominate the interactions in both the ground and the excited states, and that the dipolar solvation model will explain the spectral shifts. Indeed, the calculated direction of the shift is in agreement with predictions based on the dipole moment of the cyano radical in the ground and the excited states. In the ground state, the carbon atom bears a positive charge and water will stabilize this configuration, by appropriately orienting its dipoles and forming a hydrogen bond with nitrogen. Once the chromophore is excited from the ground state, to either the $A^2\Pi$ or the B $^2\Sigma^+$ state, the CN dipole moment flips. Now the nitrogen bears the positive charge, and the initial water configuration is

destabilizing due to the Coulomb repulsion between the positively charged nitrogen and hydrogens. Consequently, the energy gap between the ground and excited states increases with respect to the gas phase. The shift for the A state is smaller than that for the B state because the dipole moment flip is smaller. Our simulations therefore quantify the simple expectation based on dipolar solvation ideas.

As mentioned in the Introduction, our bulk simulations do not allow for electronic relaxation of water molecules upon excitation. Thus, the water charge distribution in our model is more unfavorable for the excited state than it would be in full quantum mechanical calculations. Our cluster studies indicate that this is not a major effect, but they include only a single water molecule. This effect may increase with the number of water molecules and result in a smaller blue shift. On the other hand, real water has a larger dipole moment than the computational water used, e.g., 2.35 D for SPC/E model. Consequently, greater stabilization of the ground state can be expected leading to an increased blue shift. The relative magnitude of both effects is unclear; however, the recent study by Christiansen et al.[33] demonstrated that the water electronic response effects are small. Their calculations of the n $\rightarrow \pi^*$ transition of aqueous formaldehyde employed both the nonpolarizable TIP3P and the polarizable SPCpol potentials for water in the classical MD simulations. The same water parametrizations, including polarization for SPCpol, were used in the subsequent quantum calculation of the electronic spectrum, which therefore included both electrostatic and polarization terms. The difference in the calculated vertical excitation energies is mostly due to different structures predicted in the MD simulations. When vertical excitation energies for the same set of configurations were calculated using both polarizable and nonpolarizable water, the difference was about 0.01 eV, which is much smaller than the calculated bandwidth for formaldehyde. The polarization effect may be larger in the case of the cyano radical due to greater change of the dipole moment upon excitation. However, we expect that electrostatic effects will remain dominant, as its strength is also proportional to the magnitude of the dipole moment, and that the inclusion of the electronic response would not drastically change our results.

The energies of valence repulsion and dispersion interactions depend on the size of the electronic cloud. The size of electronic density in different electronic states of CN, as defined by a gas-phase value of $\langle R^2 \rangle$, is 11.24, 11.78, and 11.57 Å^2 for the X, A and B states, respectively. Thus, weak dispersion interactions will stabilize the excited states more than the ground state. However, the valence repulsion in the excited states will be larger, due to the increased overlap between the cyano radical and water electronic density. For C_{2v} structures near the minimum, the destabilization of the excited states is almost twice as large as the stabilization of the ground state. The dipole moments in the excited states point in the opposite directions and are roughly equal to two-thirds and one-third of the ground-state dipole moment (in the B $^2\Sigma^+$ and A$^2\Pi$ states, respectively). If only electrostatic interactions were present, the potential energies would exhibit the same ratios as shown in Figure 9 by dashed lines. The remaining destabilization must, consequently, be assigned to valence repulsion, which is greater for the A$^2\Pi$ state than for the B $^2\Sigma^+$ state. Again, the C_s structures pose certain problems. Destabilization of the B $^2\Sigma^+$ state is roughly half the stabilization of the ground state. However, the A$^2\Pi$ state is actually bound but by a little less than the ground state. Extra stabilization in the full calculation may originate in additional delocalization of the π cloud across the hydrogen bond, as suggested by the calculated natural charges.

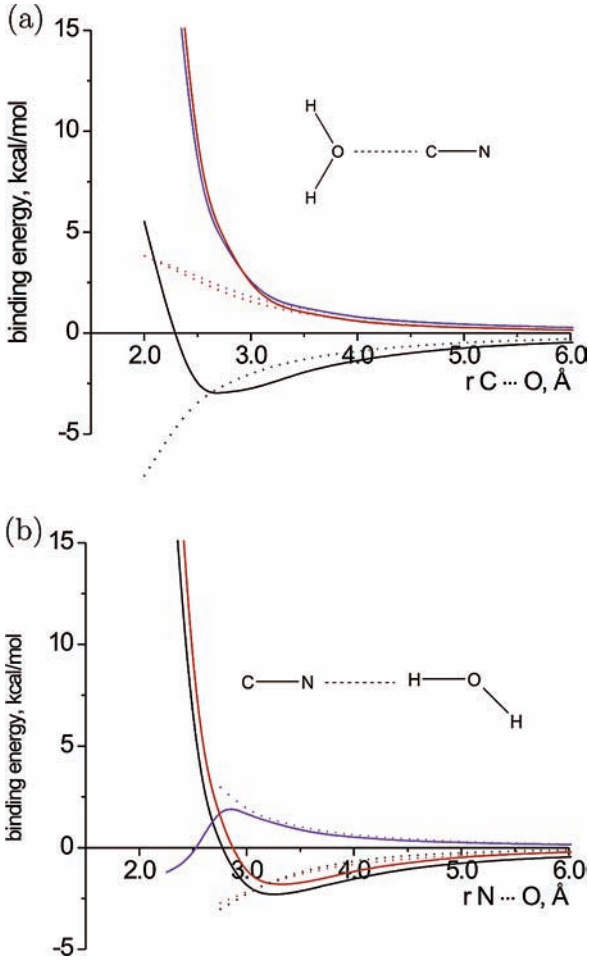

Figure 9. Potential energies of the cyano radical−water dimer in different electronic states of the cyano radical in (a) the C_{2v} symmetry and (b) the C_s symmetry structures. The lines are X $^2\Sigma^+$ CN···X$^1A_1$H$_2$O (black line), A$^2\Pi$CN···X$^1A_1$H$_2$O (red line), B $^2\Sigma^+$CN···X$^1A_1$H$_2$O (violet line). Dottted curves were obtained by replacing water with point charges derived to reproduce its gas phase dipole moment. Only the B_1 and A′ components of the A$^2\Pi$ state in C_{2v} and C_s structures are shown. The ground and excited-state energies were calculated using CCSD/6-311++G** and EOM-CCSD/6-311++G** respectively. The CP correction is not included.

In the condensed phase molecules tend to approach each other closer than the minimum of the dimer intermolecular potential. At short distances, the valence repulsion becomes very large. Let us quantify this effect and, for the sake of simplicity, concentrate on C_{2v} structures. When one moves in by 0.25 Å from the minimum on the dimer potential, the ground state now is only stabilized by ca. 2.5 kcal/mol and the excited state destabilized by ca. 9 kcal/mol. Hence, we expect that the degree of excited-state destabilization will increase in the condensed phase relative to the dimer.

To conclude, for a diatomic molecule with relatively large dipole moment in water, the electrostatic effects are dominant and, therefore, a bulk model that describes solvent by fixed point charges provides a reasonable description. Differential changes in valence repulsion and dispersion have opposing effects on the absorption shift direction; both are neglected in our approach and the magnitude of the error depends sensitively on the typical solute−solvent distances sampled at equilibrium. In the case of CN B $^2\Sigma^+ \leftarrow$ X $^2\Sigma^+$, there is a fortuitous cancellation of errors at least near the dimer minimum.

4. Conclusions

In this paper, we have described the effect of water on the electronic spectrum of the cyano radical in the bulk and in the cyano radical−water dimer. We found that, for the dimer configurations considered, the presence of water leads to a blue shift of the transitions, except for very short distances for the C_s structures. In the range that is sampled in the ground-state MD the effect of water can be reliably modeled by point charges. This significantly simplifies calculations, as this interaction enters the Hamiltonian via the one-particle part and is thus inexpensive to compute. Binding energy curves show that the size of the carbon atom, which hosts the unpaired electron, is smaller as compared to a typical saturated carbon. Thus care must be exercised when adapting typical force field parameters to model radicals in solution.

Calculations of the electronic spectrum in the condensed phase confirmed that indeed the two bands of interest exhibit a blue shift. Satisfyingly, the magnitude of the effect depends only weakly on the parametrization used in the MD part; i.e., the model sensitivity is much smaller than the bandwidth.

Let us revisit the experimental issue that motivated this work, namely the spectral assignment of the products of the ICN dissociation. Clearly, our electronic structure calculations and analysis support a moderate blue shift of the B $^2\Sigma^+ \leftarrow$ X $^2\Sigma^+$ transition of CN in water. Both EOM-CCSD and TD-DFT suggest the band center at ∼343 nm, with a wing extending to the probe wavelengths used in the experiments of Moskun et al. This supports our previous assignments.[18] In addition, new experiments have been carried out in Aarhus jointly between the Bradforth and Keiding groups to find independent evidence for an I* charge-transfer band by photodetaching $I^-_{(aq)}$. The results, however, suggest that either I* does not absorb near 315 nm as previously anticipated[21] or I* is deactivated by electronic and vibrational energy transfer on timescales much shorter than 1 ps, thus ruling out a contribution by I* detectable in the photodissociation of ICN.[66] Interestingly, the bandwidth of ∼3300 cm^{-1} and $\epsilon_{max} = 2300\ M^{-1}\ cm^{-1}$ suggested by this work[67] for the CN radical are consistent with experimental transient spectra between 220 and 380 nm that include all products from the ICN photodissociation reaction,[21] if ground-state I atoms account for the blue side and CN accounts for all absorption on the red end of the indicated range. To unambiguously confirm that CN is responsible for the 320−400 nm absorption in the experimental studies, we are carrying out a similar study based on photodetachment of $CN^-_{(aq)}$. These will provide a rigorous calibration of the theoretical models applied in this work and information on charge-transfer bands occurring in the spectrum of CN, in addition to the valence states considered here.

Acknowledgment. We thank the University of Southern California Center for High Performance Computing and Communications for making their computational resources available and technical support throughout this project. A.I.K. acknowledges the support from the National Science Foundation CAREER Award (CHE-0094116), the Alfred P. Sloan foundation, and the WISE Research Fund (USC). S.E.B. acknowledges the support from the National Science Foundation (CHE-0311814) and the David and Lucile Packard Foundation. The help of Evgueni Polikarpov (USC) in the preparation of cover graphics is gratefully acknowledged.

References and Notes

(1) Huber, K. P.; Herzberg, G. *Constants of diatomic molecules*; Van Nostrand Reinhold: New York, 1979.

(2) Hug, G. L. *Optical Spectra of Nonmetallic Inorganic Transient Species in Aqueous Solution*; U.S. Department of Commerce, National Bureau of Standards: Washington, D. C., 1981.

(3) Brocklehurst, B.; Hebert, G. R.; Innanen, S. H.; Seel, R. M.; Nicholls, R. W. The identication atlas of molecular spectra. the CN A $^2\Pi \leftarrow$ X $^2\Sigma^+$ Red System; York University, Centre for Research in Experimental Space Science, Toronto, 1971.

(4) Brocklehurst, B.; Hebert, G. R.; Innanen, S. H.; Seel, R. M.; Nicholls, R. W. The identication atlas of molecular spectra. the CN B $^2\Sigma^+ \leftarrow$ X $^2\Sigma^+$ Red System; York University, Centre for Research in Experimental Space Science, Toronto, 1972.

(5) Nadler, I.; Reisler, H.; Wittig, C. *Chem. Phys. Lett.* **1984**, *103*, 451.

(6) Nadler, I.; Mahgerefteh, D.; Reisler, H.; Wittig, C. *J. Chem. Phys.* **1985**, *82*, 3885.

(7) Casavecchia, P.; Balucani, N.; Cartechini, L.; Capozza, G.; Bergeat, A.; Volpi, G. G. *Faraday Discuss.* **2001**, *27*, 119.

(8) Ling, J. G.; Wilson, K. R. *J. Chem. Phys.* **1975**, *63*, 101.

(9) Goldfield, E. M.; Houston, P. L.; Ezra, G. S. *J. Chem. Phys.* **1986**, *84*, 3120.

(10) Dantus, M.; Rosker, M. J.; Zewail, A. H. *J. Chem. Phys.* **1987**, *87*, 6128.

(11) Benjamin, I.; Wilson, K. R. *Chem. Phys.* **1989**, *90*, 4176.

(12) Krylov, A. I.; Gerber, R. B. *J. Chem. Phys.* **1994**, *100*, 4242.

(13) Amatatsu, Y.; Morokuma, K. *Chem. Phys. Lett.* **1995**, *245*, 469.

(14) Benjamin, I. *J. Chem. Phys.* **1995**, *103*, 2459.

(15) Vieceli, J.; Chorny, I.; Benjamin, I. *J. Chem. Phys.* **2001**, *115*, 4819.

(16) Winter, N.; Chorny, I.; Vieceli, J.; Benjamin, I. *J. Chem. Phys.* **2004**, *119*, 2127.

(17) Wan, C.; Gupta, M.; Zewail, A. H. *Chem. Phys. Lett.* **1996**, *256*, 279.

(18) Moskun, A. C.; Bradforth, S. E. *J. Chem. Phys.* **2003**, *119*, 4500.

(19) Helbing, J.; Chergui, M. *J. Phys. Chem. A* **2004**, *104*, 10293.

(20) Moskun, A. C.; Jailaubekov, A. E.; Bradforth, S. E.; Tao, G.; Stratt, R. M. *Science*, in press.

(21) Larsen, J.; Madsen, D.; Poulsen, J.-A.; Poulsen, T. D.; Keiding, S. R.; Thogersen, J. *J. Chem. Phys.* **2002**, *116*, 7997.

(22) Orozco, M.; Luque, F. J. *Chem. Rev.* **2000**, *100*, 4187.

(23) Cramer, C. J.; Truhlar, D. G. *Chem. Rev.* **1999**, *99*, 2161.

(24) Luzhkov, V.; Warshel, A. *J. Am. Chem. Soc.* **1991**, *113*, 4491.

(25) Smith, P. E.; Pettitt, B. M. *J. Phys. Chem.* **1994**, *98*, 9700.

(26) Gao, J.; Byun, K. *Theor. Chim. Acta* **1997**, *96*, 151.

(27) Bradforth, S. E.; Jungwirth, P. *J. Phys. Chem. A* **2002**, *106*, 1286.

(28) Winter, N.; Chorny, I.; Vieceli, J.; Benjamin, I. *J. Chem. Phys.* **2003**, *119*, 2127.

(29) Mercer, I. P.; Gould, I. R.; Klug, D. R. *J. Phys. Chem. B* **1999**, *103*, 7720.

(30) Warshel, A.; Levitt, M. *J. Mol. Biol.* **1976**, *103*, 227.

(31) Thompson, M. A.; Schenter, G. K. *J. Phys. Chem.* **1995**, *99*, 6374.

(32) Kongsted, J.; Osted, A.; Mikkelsen, K. V.; Christiansen, O. *Mol. Phys.* **2002**, *100*, 1813.

(33) Kongsted, J.; Osted, A.; Mikkelsen, K. V.; Astrand, P. O.; Christiansen, O. *J. Chem. Phys.* **2004**, *121*, 8435.

(34) Gordon, M. S.; Freitag, M. A.; Bandyopadhyay, P.; Jensen, J. H.; Kairys, V.; Stevens, W. J. *J. Phys. Chem. A* **2001**, *105*, 293.

(35) Bandyopadhyay, P.; Gordon, M. S.; Mennucci, B.; Tomasi, Jacopo *J. Chem. Phys.* **2002**, *116*, 5023.

(36) Krauss, M. *Comput. Chem.* **1995**, *19*, 33.

(37) Case, D. A.; Darden, T. A.; Cheetham, T. E., III; Simmerling, C. L.; Wang, J.; Duke, R. E.; Luo, R.; Merz, K. M.; Wang, B.; Pearlman, D. A.; Crowley, M.; Brozell, S.; Tsui, V.; Gohlke, H.; Mongan, J.; Hornak, V.; Cui, G.; Beroza, P.; Schafmeister, C.; Caldwell, J. W.; Ross, W. S.; Kollman, P. A. *Amber 8, University of California, San Francisco* **2004**.

(38) Kong, J.; White, C. A.; Krylov, A. I.; Sherrill, C. D.; Adamson, R. D.; Furlani, T. R.; Lee, M. S.; Lee, A. M.; Gwaltney, S. R.; Adams, T. R.; Ochsenfeld, C.; Gilbert, A. T. B.; Kedziora, G. S.; Rassolov, V. A.; Maurice, D. R.; Nair, N.; Shao, Y.; Besley, N. A.; Maslen, P.; Dombroski, J. P.; Daschel, H.; Zhang, W.; Korambath, P. P.; Baker, J.; Bird, E. F. C.; Van Voorhis, T.; Oumi, M.; S. Hirata, C.-P. Hsu; Ishikawa, N.; Florian, J.; Warshel, A.; Johnson, B. G.; Gill, P. M. W.; Head-Gordon, M.; Pople, J. A. *J. Comput. Chem.* **2000**, *21*, 1532.

(39) Stanton, J. F.; Gauss, J.; Watts, J. D.; Lauderdale, W. J.; Bartlett, R. J. *ACES II* **1993**. The package also contains modified versions of the MOLECULE Gaussian integral program of J. Almlöf and P. R. Taylor, the ABACUS integral derivative program written by T. U. Helgaker, H. J. Aa. Jensen, P. Jørgensen and P. R. Taylor, and the PROPS property evaluation integral code of P. R. Taylor.

(40) Thomson, R.; Dalby, F. W. *Can. J. Phys.* **1968**, *46*, 2815.

(41) Purvis, G. D.; Bartlett, R. J. *J. Chem. Phys.* **1982**, *76*, 1910.

(42) Raghavachari, K.; Trucks, G. W.; Pople, J. A.; Head-Gordon, M. *Chem. Phys. Lett.* **1989**, *157*, 479.

(43) Watts, J. D.; Gauss, J.; Bartlett, R. J. *J. Chem. Phys.* **1993**, *98*, 8718.

(44) Cristian, A. M. C.; Shao, Y.; Krylov, A. I. *J. Phys. Chem. A* **2004**, *108*, 6581.
(45) Becke, A. D. *J. Chem. Phys.* **1993**, *98*, 5648.
(46) Kendall, R. A.; T. H. Dunning, Jr.; Harrison, R. J. *J. Chem. Phys.* **1992**, *96*, 6796.
(47) Krishnan, R.; Binkley, J. S.; Seeger, R.; Pople, J. A. *J. Chem. Phys.* **1980**, *72*, 650.
(48) Clark, T.; Chandrasekhar, J.; Schleyer, P. V. R. *J. Comput. Chem.* **1983**, *4*, 294.
(49) Boys, S. F.; Bernardi, F. *Mol. Phys.* **1970**, *19*, 553.
(50) This approach is not strictly correct as the ROHF reference is not formally size-consistent. However, the introduced error is numerically negligible.
(51) Sekino, H.; Bartlett, R. J. *Int. J. Quantum Chem. Symp.* **1984**, *18*, 255.
(52) Stanton, J. F.; Bartlett, R. J. *J. Chem. Phys.* **1993**, *98*, 7029.
(53) Runge, E.; Gross, E. K. U. *Phys. Rev. Lett.* **1984**, *52*, 997.
(54) Hirata, S.; Head-Gordon, M. *Chem. Phys. Lett.* **1999**, *314*, 291.
(55) Lovas, F. J. *J. Phys. Chem. Ref. Data* **1978**, *7*, 1445.
(56) Berendsen, H. J. C.; Grigera, J. R.; Straatsma, T. P. *J. Phys. Chem.* **1987**, *91*, 6269.
(57) NBO 4.0. Glendening, E. D.; Badenhoop, J. K.; Reed, A. E.; Carpenter, J. E.; Weinhold, F. Theoretical Chemistry Institute, University of Wisconsin, Madison, WI, 1996.
(58) Rick, S. W. *J. Chem. Phys.* **2004**, *120*, 6085.
(59) Mahoney, M. W.; Jorgensen, W. L. *J. Chem. Phys.* **2000**, *112*, 8910.
(60) Berendsen, H. J. C.; Postma, J. P. M.; van Gunsteren, W. F.; DiNola, A.; Haak, J. R. *J. Chem. Phys.* **1984**, *81*, 3684.
(61) Cornell, W. D.; Cieplak, P.; Bayly, C. I.; Gould, I. R.; Merz, K. M.; Ferguson, D. M.; Spellmeyer, D. C.; Fox, T.; Caldwell, J. W.; Kollman, P. A. *J. Am. Chem. Soc.* **1995**, *117*, 5179.
(62) Wang, B.; Hou, H.; Gu, Y. *Chem. Phys. Lett.* **1999**, *303*, 96.
(63) Cook, T. J.; Levy, D. H. *J. Chem. Phys.* **1973**, *59*, 2387.
(64) Tozer, D. J.; Amos, R. D.; Handy, N. C.; Roos, B. O.; Serrano-Andres, L. *Mol. Phys.* **1999**, *97*, 859.
(65) Bayliss, N. S.; McRae, E. G. *J. Phys. Chem.* **1954**, *58*, 1002.
(66) Moskun, A.C; Bradforth, S. E.; Thogersen, J.; Keiding, S. *J. Phys. Chem. A*, submitted for publication.
(67) The extinction coeffiction has been calculated using the experimental oscillator strength of the cyano radical in the gas phase ($f = 0.033$) and the bandwidth computed using Set B+TIP5P/E ($\nu_{1/2} = 3300$ cm^{-1}) by using:[1] $\epsilon_{max}(M^{-1}\ cm^{-1}) = 2.31 \times 10^8 f \nu_{1/2}^{-1}$.